Chaotic signal generation using photonic techniques

Author: Juan Antonio Lloret Soler

Supervisor: Dr. Francisco Ramos Pascual

Resumen — Junto con satisfacer la creciente demanda a ser soportada por las redes de datos en términos de capacidad, la seguridad de la información en las comunicaciones también se ha convertido en un tema que ha atraído el interés de los investigadores en los últimos años. Muchas han sido las soluciones planteadas hasta la fecha. Entre ellas y, debido a sus características inherentes, los sistemas basados en caos se presentan como el complemento perfecto de las soluciones más utilizadas actualmente, siendo éstas la criptografía cuántica y la encriptación soportada por software. Ello, tiene como objetivo reportar un alto valor añadido al grado de seguridad ya establecido por dichas soluciones. En este trabajo, se presenta una estructura novedosa formada por un SOA-MZI con bucle de realimentación, cuyo objetivo es el de desarrollar funcionalidades propias de un generador de señal caótica. El estudio del comportamiento de la estructura se realiza en función de sus parámetros físicos más importantes a partir principalmente del cálculo del Exponente Global de Lyapunov (GLE).

Abstract — Together with providing larger capacities in data networks with the aim at fulfilling the increasing demand, security has become an important issue which has intensively attracted the researchers' attention in the last years. In order to deal with this issue, several solutions have already been presented so far. Among them, due to their inherent characteristics, chaos-based systems have arisen as the perfect complement to the most extensively used solutions, as the quantum cryptography and the software encryption are. In this work, a novel all-optical structure based on a single SOA-MZI with feedback loop is presented for the purpose of acting as a chaotic carrier generator. The performance of the structure is mainly characterized in terms of the Global Lyapunov Exponent (GLE) as a function of the most important physical parameters.

Author: Juan A. Lloret, email: jualloso@iteam.upv.es
Supervisor: Dr. Francisco Ramos, email: framos@dcom.upv.es
Due date: 24-03-10

CONTENTS

I. Overview

In the last decades, an exponential growth of the demanded bandwidth per final network user has been experienced. It means that data networks have to be able to process high bitrates in order to satisfy a certain quality of service.

Historically, the electronic technology has been employed to process optical signals. Nowadays, electronic devices are becoming a bottleneck in optical networks owing to their narrow bandwidth compared to the capacity available in the optical systems. The aforementioned limitation can be overcome by implementing all-optical data processing networks. Devices based on optical technology establish a series of advantages that cannot be overlooked. These advantages mainly consist of the huge bandwidth which they are capable of supporting and the transparency regarding the data bitrates, the data format, and the transmission encoding. Moreover, other inherent characteristics of optics can be also exploited like, for instance, electromagnetic interference immunity, absence of impedance-matching problems and low skew and weight.

Equally important as the increase of processing capacity, is the fact of providing secure communications and information exchanges. Due to the nature of the optical link, it becomes difficult to tap by an eavesdropper; but certainly possible. Furthermore, in multiplexed systems where several users are sharing the physical medium, it is of great importance to provide high degree of privacy by isolating the information addressed to the receiver from the rest of the network users. In scenarios like these, chaos plays an important role with the aim at increasing the value added of secure transmissions.

In 1963, Edward Lorentz was the first one in observing strange aperiodic behavior in a three-dimensional system [1]. In the beginning, it was desirable to avoid this sort of behavior, because it was associated to system instabilities. However, in the eighties, researchers start realizing how chaos could be used as a very powerful tool in order to implement secure solutions at the hardware level in data networks. To develop functionalities directly at the physical layer allows the system to fully exploit the advantages of the photonic technology, relying on an important issue to be considered when implementing the security subsystems in data networks.

The issue of communication secrecy has served as an important motivation for research involving communications with chaos. Much of this research has sought to use chaotic signals as a means of sending secret messages. Certainly, fundamental properties of chaotic systems seem to make them ideal for this purpose. Chaotic systems are inherently unpredictable because their dynamics are aperiodic and irregular [2]. The following figure clearly shows the basic concept of chaotic-based secure communications. In which, a message is added to or modulated onto unpredictable behavior generated by the chaotic system at the transmitter. Once the message reaches the receiver, it becomes necessary to efficiently separate the unpredictable behavior from

the valid information. For this purpose, a second chaotic system identical to the first must be perfectly synchronized to the transmitter.

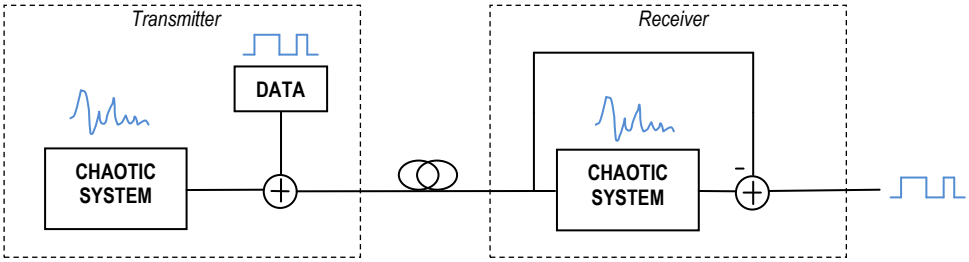

Fig. 1. Basic concept of chaotic-based transmission system.

According to the pioneering of the secrecy in data transmissions, Claude Shannon, an efficient secret communication system must respect three important aspects: concealment, privacy, and encryption [3]. These aspects can be interpreted in the context of chaotic communications. By concealment, Shannon refers to such methods as invisible ink in which the existence of the message is concealed from an eavesdropper. Concealment of a message using chaotic carrier signals is possible due to their aperiodic and irregular behavior, so the presence of a message in the chaotic fluctuations may not be obvious. Regarding the second aspect, communication privacy, occurs in systems in which special equipment is required to recover the message. This situation is present in chaotic communication systems since an eavesdropper must have a proper receiver, with matched parameter settings to decode the message. Finally, encryption occurs naturally in chaotic communication techniques. In conventional encryption techniques, a "key" is often used to encrypt the message. If the transmitter and receiver share the same key, the scrambled message can be recovered by the receiver. In chaotic systems, the transmitter itself acts as a "dynamical key" depending on the initial conditions and setting parameters of the system.

As a result, nowadays optical chaos encryption has arisen as a promising and efficient technique in order to implement secure communications. The purpose of chaos does not consist of displacing existing technologies like quantum cryptography or software-based solutions, but act as a complement of them with the aim at increasing the data privacy and security in optical and hybrid networks [4, 5].

I.1. *Pursued objectives.*

The main objective of the present work is to design and characterize an all-optical structure which can act as a chaotic carrier generation. The structure must allow being routed to chaotic behavior by means of adjusting the proper setting parameters subject to certain initial conditions. It is also highly desirable to define controllable parameters, whose status can govern the nature, chaotic or not chaotic, of the system's output. In order to meet the above-mentioned objectives, the present work addresses the following separate goals:

- To gain good understanding of the basic concepts involving the chaos theory.
- To fully understand the advantages and limitations of the chaos-based communications secure systems with respect to more popular solutions, like software encryption or quantum cryptography, as well as its possible market role.
- To develop an accurate analytical description of the proposed structure for the purpose of performing stability studies and numerical calculations.
- To implement a generic algorithm with the functionality of calculating a relevant enough indicator of chaotic dynamics.
- To find out the values of the controllable parameters that yield chaotic behavior to give proper support in the design's stage of the architecture, as well as to define the optimum solutions in terms of the performance.

I.1. *Introduction.*

Investigations carried out in the present work focuses on studying the chaotic behavior induced by a novel all-optical structure based on a single SOA-MZI with optical feedback. The structure can be routed to complex dynamics by exploiting nonlinear effects in the semiconductor waveguides, which are magnified by means of the feedback loop.

The work reported in the present document is split into 5 mainly sections. Firstly, section I depicts important theoretical concepts and background necessary in order to make this work as outstanding as possible. Following, section II gives brief comments about the current state-of-the-art in this field, as well as about the proposed system. Section III focuses on presenting the analytical description developed for the purpose of accurately modeling the proposed system. In addition, stability studies when considering static and dynamic behavior are performed. On the other hand, section IV contains the numerical results of the Global Lyapunov Exponent (GLE) depending on some of the most important system parameters. Finally, section V summarizes the main conclusions obtained and some suggestions regarding further investigations that could be interesting on this device are given as well.

I.2. *Definition of Chaos.*

Chaos is defined as an aperiodic long-term behavior in a deterministic system that exhibits sensitive dependence on initial conditions [2]. The three components which made the definition up are clarified as follows:

Aperiodic long-term behavior means that the system's trajectory in the phase space does not settle down to any fixed points (steady state), periodic orbits or quasi-periodic solutions as time tends to infinity. This part of the definition differentiates aperiodicity due to chaotic dynamics from the transient aperiodicity of, for example, a periodically oscillating system that has been momentarily perturbed.

Deterministic system can allow no stochastic parameters. It is a common misconception that chaotic systems are noisy driven by chaos processes. The irregular behavior of chaotic systems arises from intrinsic nonlinearities rather than noise. As any deterministic system, chaos is predictable on a short time scale, whereas on a long time scale, chaotic systems become unpredictable.

Sensitive dependence on initial conditions requires that trajectories originating from very nearly identical initial conditions will diverge exponentially quickly. For the same system, small differences in the initial conditions yield large differences in the long-run behavior.

I.3. *How to measure chaos.*

The chaotic behavior of a system can be characterized according to both the geometrical and the dynamical aspects of its attractor.

Firstly, it must be mentioned that the geometrical representation of the system's solution with the time is known as *phase space*. Loosely speaking, an *attractor* is a subset of the phase space of a dissipative dynamical system that "attracts" phase points from other regions of the phase space in the basin of the attractor. Once a phase point enters an attractor, it does not leave it. There exists different kind of attractors and they can be classified as: fixed points, limit cycles, two-dimensional toris and strange attractors. In case of presenting the attractor chaotic behavior, then it is called *strange attractor* [6]. Figure 2 shows some examples of different kind of attractors for two-dimensional systems.

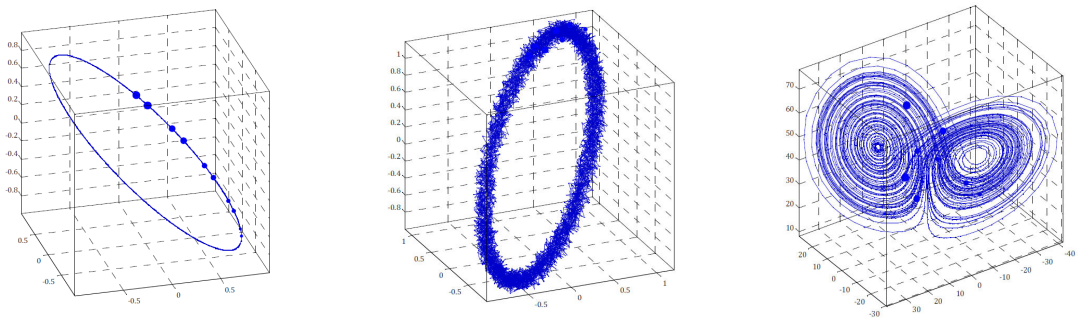

(a) (b) (c)

Fig. 2. Examples of different attractors. (a) Limit cycle. (b) Noisy two-dimensional tori. (c) Strange attractor (Lorentz attractor).

As it will be shown in section III, the analytical description of the proposed system is based on a set of delay nonlinear differential equations. It means that the current state of the system also depends on past-time states, as one can see in the general description given by (1).

$$\frac{dx(t)}{dt} = F\left[x(t), x(t-\tau)\right] \tag{1}$$

A delay differential equation is found to be *infinite-dimensional*, since an infinite set of numbers along the time τ is needed in order to completely define the initial condition. To simulate the behavior of infinite-dimensional systems, it is necessary to approximate the continuous evolution of an infinite-dimensional system by a finite number of elements whose values change at discrete time steps. In this manner, a continuous infinite-dimensional system is replaced by a finite-dimensional iterated map. Hence, the theory of finite-dimensional dynamical systems can be applied. The number of independent real numbers that are needed to specify an arbitrary initial condition is called the *phase space dimension (N)* [6].

On the other hand, the number of degrees of freedom is known as *embedding dimension (M)*. In general, to gain geometric picture of an N-dimensional system, all N coordinates must be taken into account. However, if an attractor has embedding dimension $M<N$, only M variables are needed to determine a trajectory on the attractor.

In order to study the chaotic behavior of a certain system, several indicators have been reported in the literature. Among them, three are the most important due to their wider application field. Specifically, these are the *fractal dimension*, the *metric entropy* and the *spectrum of Lyapunov exponents*. The last one has been the most commonly used to measure the strangeness of attractors in the last years. In the beginning, however, the fractal dimension was extensively used because it requires less computation capacity. Following, brief comments about the three methods are given.

I.3.1. *Fractal dimension.*

For a dynamical system with an N-dimensional phase space, let $n(\varepsilon)$ be the number of N-dimensional balls of radius ε required to cover an attractor. So, the fractal dimension (also known as capacity) of a dynamical system is defined as [6],

$$D_F = \lim_{\varepsilon \to 0} \frac{\log[n(\varepsilon)]}{|\log[\varepsilon]} \tag{2}$$

Strange attractors are typically characterized by fractal dimensionality D_F which is smaller than the number of degrees of freedom, or equivalently, the embedding dimension M of the system, $D_F<M$. Several attempts to compute this number directly from box-counting algorithms, which stem from the definition of this dimensionality, have been presented [7, 8]. However, it turns out that it is very difficult or impractical to compute D_F whenever $D_F>2$ [9].

In 1982, P. Grassberger and I. Proccacia suggested a different measure for the strangeness of attractors, a measure which can be easily performed from any time series, which is closely related to the fractal dimension. Indeed, in many cases, this measure is more relevant at the time of characterizing chaotic behavior than the fractal dimension itself [10]. The measure is obtained by

considering correlations between points of a long-term time series on the attractor. Specifically, the *k* points of such a long-time series are denoted by:

$$\left\{\vec{X}_i\right\}_{i=1}^{k} = \left\{\vec{X}_i\left(t+i\sigma\right)\right\}_{i=1}^{k}, \tag{3}$$

where σ is an arbitrary but fixed time step increment. On the other hand, the standard correlation integral in the discrete time domain is defined as follows.

$$C\left(r\right) \equiv \lim_{k\to\infty} \frac{1}{k^2} \sum_{i,j=1}^{k} \theta\left(r - \left| \vec{X}_i - \vec{X}_j \right| \right) \tag{4}$$

Being *θ(x)* the Heavisade step function, where *θ(x)=1* if *x≥0* and *θ(x)=0* if *x<0*. The main point is that *C(r)* behaves as a power of *r* when considering *r* small enough.

$$C\left(r\right) \propto r^{v} \tag{5}$$

The exponent *v* is closely related to D_F. Both parameters normally only differs few hundredths and they always follow the relation $v \leq D_F$. Hence, the slope of the correlation integral establishes an excellent estimate of the fractal dimension of a strange attractor.

By considering the definition depicted in (2), the regions of the attractor which are rarely visited contribute to D_F with identical weight as regions characterized by high visiting rate. The correlation integral, however, is sensitive to this effect. In this sense *v* may be a more relevant measure of the strangeness than D_F, because it is sensitive to the dynamical process of coverage of the attractor. So, the difference between *v* and D_F gives a measure of the importance of the different seniority of diverse neighborhoods.

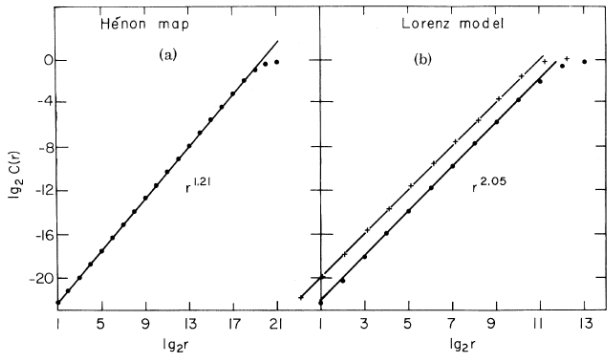

Fig. 3. Computed correlation integrals. (a) Hénon map. (b) Lorentz model. Both traces in (b) are obtained by taking into account two different values of the time step σ [10].

In figure above, an example of the computation of the correlation integral plotted on log-log scale is shown for the Hénon map and the Lorentz system. One can clearly see how the correlation integral presents linear behavior with an arbitrary scale of *r*. In order to decide if the attractor is characterized or not by chaotic aperiodicity, the exponent of the power-law must be compared with the embedding dimension of the system. Specifically, *M* is 2 for the Hénon map and 3 for the Lorentz model. Therefore, both attractors are found to be chaotic in the case under study, since fractal dimensions of approximately 1.21 and 2.05 are obtained respectively, fulfilling that $D_F<M$.

I.3.2. *Metric entropy.*

One of the essential differences between chaotic and predictable behavior is that chaotic trajectories continually generate new information, whereas predictable trajectories do not. The metric entropy makes this notion precise. Moreover, the metric entropy not only provides good definition of chaos, but also provides a quantitative way to describe how chaotic a dynamical system is [6].

For proper definition of the metric entropy, suppose a phase space partitioned into *n* elements, each of which is assigned a symbol s_i. Consider a sequence $S_j(m)$ of *m* successive measurements made at a time interval Δt, $S_j(m)=\{s_{i1}, s_{i2}, \ldots, s_{im}\}$. Let $P(S_j(m))$ be the probability of the sequence $S_j(m)$ normalized, it means $\Sigma_j P(S_j(m))=1$. Then, the amount of information contained in sequences of length *m* can be expressed as [6]:

$$I_m = -\sum_j P\left(S_j(m)\right)\log\left(P\left(S_j(m)\right)\right) \tag{6}$$

By taking the maximum value over all the possible partitions, the metric entropy h_μ is defined as the information per time unit in a sequence of measurements [6].

$$h_\mu = \sup\left\{\frac{I_m}{m\Delta t}\right\} \tag{7}$$

For predictable dynamical systems, eventually new measurements provide no further new information, and the metric entropy is zero. However, for chaotic dynamical systems new measurements continue providing new information, giving as a result positive metric entropy.

As defined, the metric entropy depends on the set of probabilities $P(S_j(m))$. This in turn may depend on the choice of initial conditions. So, special care must be taken at the time of choosing the initial condition. More complete discussions regarding this issue can be found in [11].

I.3.2. *Lyapunov exponents.*

The spectrum of Lyapunov characteristic exponents provides good knowledge of the local stability properties of a certain attractor.

The stability properties of a system are determined by studying its behavior under small perturbations. It must be highlighted that a system can be stable to perturbations in certain directions, yet be unstable to perturbations in others. All possible perturbations can be examined simultaneously by following the evolution of an ensemble of points that is initially contained in a small N-dimensional ball, where N is the dimension of the phase space [6]. This motivates the concept of spectrum of Lyapunov exponents.

Consider an N-dimensional dynamical system. It is well-known that two different initial conditions will report two different orbits on the phase space. Take one of them as a reference orbit. Following, imagine an infinitesimal ball which is characterized by radius $\varepsilon(0)$ at time $t=0$ and centered enclosing both initial conditions of both orbits. As time goes on, the ball evolves under the action of the non-uniform flow described by the dynamical system, and it will be distort because the separation between both orbits is time-dependent. The shape's change of the ball is mainly determined by the linear part of the flow, which means that the ball remains as a sort of ellipsoid as it evolves. Let call the axis of this ellipsoid at time t $\varepsilon_i(t)$ where $i \in [1,N]$. So, the spectrum of Lyapunov exponents λ_i for a given starting point is [6]

$$\lambda_i = \lim_{t\to\infty}\left[\lim_{\varepsilon(0)\to 0}\left(\frac{1}{t}\log\left(\frac{\varepsilon_i(t)}{\varepsilon(0)}\right)\right)\right] \tag{8}$$

From the definition, it must be noticed that there exists N Lyapunov exponents in the spectrum of an attractor of an N-dimensional dynamical system for a given starting point. Positive Lyapunov exponents measure average exponential spreading of nearby trajectories, and negative exponents measure exponential convergence of trajectories onto the attractor. Note that the sum of Lyapunov exponents is the average divergence, which for a dissipative system must be always negative [6]. The largest Lyapunov exponent, $\lambda=sup_i\{\lambda_i\}$, is called *Global Lyapunov Exponent (GLE)*, and the information which reports is especially useful for distinguishing among the various types of orbits:

$\lambda<0$: The orbit attracts to a stable fixed point or stable periodic orbit. Negative Lyapunov exponents are characteristic of dissipative or non-conservative systems. Such systems exhibit asymptotic stability; the more negative the exponent, the higher the stability. Super-stable fixed points and super-stable periodic orbits have a GLE of $\lambda=-\infty$ [12].

$\lambda=0$: The orbit is a neutral fixed point (or an eventually fixed point). It indicates that the system is in a sort of steady state mode, so it is found to be conservative but close to the "transition to chaos" [12].

$\lambda>0$: The orbit present unstable and chaotic behavior. Nearby points, no matter how close they may be, will diverge to any arbitrary separation. All neighborhoods in the phase space will eventually be visited. These points are said to be unstable [12].

For estimating the GLE, two main methods have been published in the literature so far. On one hand, the first one was proposed by *Wolf et al.* in 1985 and it is based on the *direct approach*. The direct approach consists of tracing the exponential divergence of nearby trajectories. It must be mentioned that this approach is subject to many critics, because it requires long data series and is sensitive to dynamic noise. On the other hand, the second one was proposed by *Eckmann & Ruelle* in 1985 and, in this case, it is based on a *Jacobian approach* [12]. By using the derivatives instead of the data series directly obtained from the solutions of the dynamical system, has important advantages in terms of accurately estimating the GLE even in presence of moderate noise.

From the Lyapunov spectrum, it can be characterized both the geometrical and the dynamical aspects of a strange attractor. The first one can be accomplished by computing the Kaplan-Yorke dimension or the Mori dimension. On the other hand, the second one can be obtained by calculating the Kolmogorov-Sinai entropy.

I.3.2.1. *Kaplan-Yorke and Mori dimensions.*

Two conjectures have been put forth to define the dimension of the dynamical system from the spectrum of Lyapunov exponents.

In first place, according to the conjecture of Kaplan-Yorke, the information dimension with the Lyapunov exponents is related to as follows.

$$D_{KY} = j + \frac{\sum_{i=1}^{j} \lambda_i}{\left|\lambda_{j+1}\right|} \tag{9}$$

Where j is the largest integer for which the relationship $\lambda_1+\lambda_2+...\lambda_j \geq 0$ is obeyed. It represents a measure of the degree of disorder of the points on the attractor [13].

Secondly, Mori conjectured that the fractal dimension of an attractor may be related to the spectrum of Lyapunov exponents as [14]:

$$D_M = d + \frac{\sum_{i=1}^{k} \lambda_i^{+}}{\sum_{i=1}^{l} \left|\lambda_i^{-}\right|} \tag{10}$$

Where d is the number of non-negative exponents, k is the number of positive exponents λ_i^{+}, and l is the number of negative exponents λ_i^{-}.

Both conjectures will report the same result in the case of continuous dynamical systems of embedding dimensions three or less, or in the case of discrete dynamical systems of embedding dimension two or less [6].

I.3.2.2. *Kolmogorov-Sinai entropy.*

The degree of chaos of a system can be measured from a generalization of the concept of entropy for state space dynamics. Loosely speaking, the Kolmogorov-Sinai entropy measures the average loss of the information rate. So, it is inversely proportional to the time interval over which the future evolution can be predicted [15].

The computation of the Kolmogorov-Sinai entropy may be performed from the spectrum of Lyapunov exponents through the so-called Pesin identity, which states that

$$h_{KS} = \sum_i \lambda_i \tag{11}$$

Where the index i makes only reference to those Lyapunov exponents which obey that $\lambda_i > 0$. To be precise, the sum of the positive Lyapunov exponents is an upper bound to the Kolmogorov-Sinai entropy, but (11) seems to hold in very general situations and it is usually the only way to obtain a good estimation of h_{KS} [15]. The important point here is that the larger the entropy, the larger the unpredictability of the system, which is a highly desired property to ensure security in a chaos encryption scheme.

II. State-of-the-art and proposed system

Once a capacity large enough for guaranteeing short and medium-term applications requirements is provided by the telecommunication networks, the next big challenge is focused on the development of security communications. Up until now, much of scientists' efforts have actively been on software coding methods, such as the well-known public-key cryptography. However, researchers are also developing other promising techniques which operate at the physical level.

Among these, quantum cryptography has arisen as the preferred solution, with some commercial systems already available. Nevertheless, the potential of chaotic signals as a powerful complement to quantum cryptography has intensively attracted the researchers' attention. Now, after more than a decade of investigation, optical chaotic cryptography is approaching the market.

Several solutions for implementing chaotic-based communication systems have already been reported in the literature [15-17]. In the beginning, hybrid solutions by using both electronic and photonic technologies were suggested. However, communication networks tend toward all-optical technologies, so the future passes through designing integrated all-optical robustness solutions.

All the solutions reported can be classified attending to the encryption techniques implemented in the transmitters, as well as the topology of the receivers.

II.1. *Encryption techniques in the transmitter.*

The transmitter of a chaotic-based communication system is made up by a subsystem which may be routed to chaotic behavior under certain conditions. Transmitters can be classified according to the method used for combining chaos and message. Historically, all encryption techniques have been based on amplitude modulation (AM) of the chaotic carrier, and there mainly exists three different techniques as shown in Fig. 4.

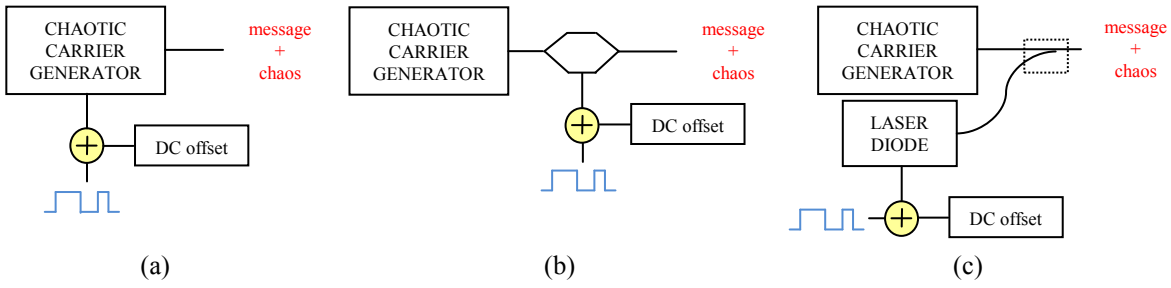

Fig. 4. Encryption techniques. (a) Chaos shift keying. (b) Chaos modulation. (c) Additive chaos masking.

In the basic scheme, the chaotic carrier is simply superposed over the message to strongly reduce its signal-to-noise ratio, thus implementing the so-called *additive chaotic masking*, as shown in Fig. 4 (c). Another possible approach is to superpose the message to the pump current of the laser by direct modulation, being referred as *chaos shift keying* (Fig. 4 (a)). Finally, other scheme consist of modulating in amplitude the light beam emitted by the chaotic carrier generator

by means of an electro-optical modulator, sketched in Fig. 4 (b), which is known as *chaos modulation*. More complex structures based on phase modulation (PM) by using an in-cavity phase modulator are also possible [18].

Figure 5 shows a real-implemented all-optical integrated module which acts as an entire transmitter. It is mainly made up by a DFB laser provided by an external cavity, which develops the functionality of chaotic carrier generator. The cavity is composed by a SOI waveguide, which is terminated by a highly reflective mirror (HR) in one of both sides. The message is modulated in phase by means of a phase modulator and the amplitude of the feedback signal injected into the DFB again is controlled by a variable optical attenuator (VOA). By employing integrated solutions, better mechanical stability, lower temperature sensitivity, and more compact and rugged systems can be achieved at lower volume cost.

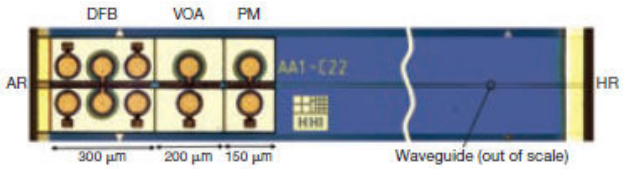

Fig. 5. Top view of all-optical integrated module for chaos-based transmission [18].

II.2. *Open and close loop receivers.*

Two possible configurations have been presented so far in the literature in order to design a proper receiver able to extract the message from the chaotic carrier. Specifically, both architectures proposed are based on the same idea, which is to reproduce the chaotic carrier at the receiver for the purpose of subtracting it from the transmitted signal. However, both architectures carry this objective out in a different way.

On one hand, the so-called close-loop configuration consists of a totally symmetric scheme used in the transmitter and in the receiver. It means that the receiver is chaotic by itself, even without injection (Fig. 6 (a)).

On the other hand, the receiver in a scheme based on open-loop configuration is not subject to feedback. Hence, the receiver is not chaotic in the absence of the transmitted signal (Fig. 6 (b)).

Earlier studies have shown that the open-loop configuration leads to synchronization more readily than the closed-loop one. Furthermore, the close-loop architecture requires careful tuning of the feedback phase to adjust it in a similar way for both the transmitter and the receiver [19].

The dependence of implementing different decoding processes at the receiver on the fidelity of the recovered signal has also been object of study in the literature. Specifically, two major decoding techniques have focused the interests of researchers. The first one relies on the widely proposed process based on subtracting the chaotic carrier from the received signal directly in the optical domain, which is known as *normalized difference of electric fields*. However, the second

one corresponds to a more realistic case and it is extensively used under "real-world" conditions, as well as in experimental set-ups. The *subtraction of photocurrents*, as it is known the above-mentioned decoding process, is based on subtracting the electrical current outputs of a pair of photodiodes (see Fig. 6). The normalized difference of electric fields technique is found to be less complex than the subtraction of photocurrents, because a lower number of devices are needed. Moreover, the processing is completely implemented on the optical layer. Nevertheless, especially when using close-loop configurations, this technique becomes strictly dependent on the degree of synchronization between the transmitter and the receiver. That is the reason why the subtraction of photocurrents decoding process is commonly used in order to overcome the above-mentioned limitation independently of the receiver topology [20].

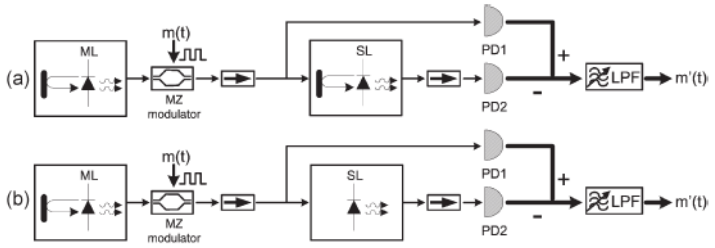

Fig. 6. Two different communications chaos-based schemes characterized by close-loop receiver configuration (a) and by open-loop receiver configuration (b) [20].

Finally, it must be highlighted that some years ago the first test under real-world conditions chaos-based communication was performed [19]. The test was carried out by making use of commercial devices strictly. It consisted of transmitting a message embedded within optical chaos along a 120 km optical link based in the metropolitan optical network of Athens. Successful results in terms of bit error rate (BER) were achieved. To avoid problems related to fiber dispersion, compensation modules made up by proper length dispersion-shifted fibers were utilized. This is issue becomes important because otherwise, the receiver could not correctly synchronize with the transmitted signal due to temporal repercussions on the signal induced by the fiber dispersion. Moreover, high order effects were also avoided thanks to the use of single-mode optical links, as well as the use of distributed feedback (DFB) lasers. Both the set-up tested and the performance achieved by the system is shown in Fig. 7.

In Fig. 7(a), one can see how the decoded message and the input one are practically identical. It must be noticed that the electric voltage level is roughly the same, issue which has been possible by using an erbium doped fiber amplifier (EDFA) pumped with the proper power at the transmitter's output in order to compensate the propagation losses of the optical link. Fig. 7(b) also shows that the fact of taking into account the fiber link and larger code lengths slightly penalize the BER as a function of the bit rate, but the penalization is not so important. Therefore,

the results obtained by the test provide a convincing proof-of-practical-concept for optical chaos communications. Building on this, it should be possible to develop reliable cost-effective secure communications systems for the purpose of being implanted in real networks [19].

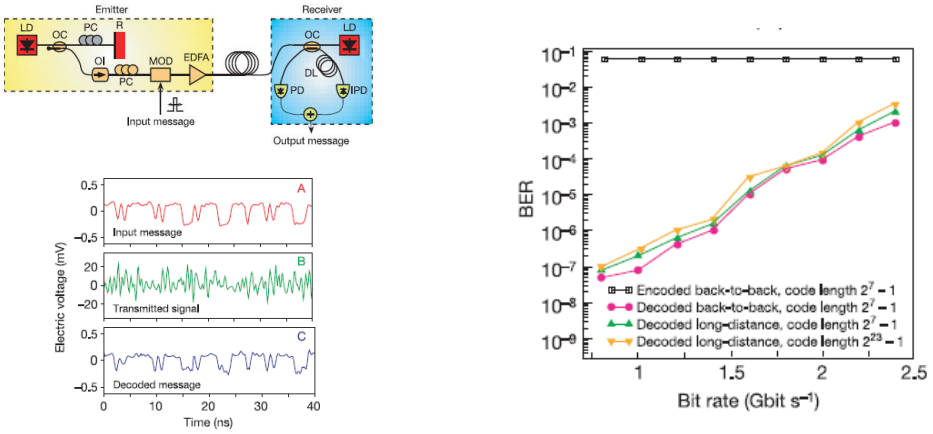

(a) (b)

Fig. 7. (a) Set-up and temporal waveforms of the input and decoded message, and transmitted signal (message + chaos). (b) BER performance of different scenarios and code lengths [19].

II.4. *Proposed system based on SOA-MZI with optical feedback.*

In this section, a novel all-optical structure which can act as optical carrier generator under certain initial conditions and proper setting parameters is presented. Specifically, the structure is based on a semiconductor-optical-amplifier-based Mach-Zehnder interferometer with optical feedback loop, as one can see in Fig. 8(a).

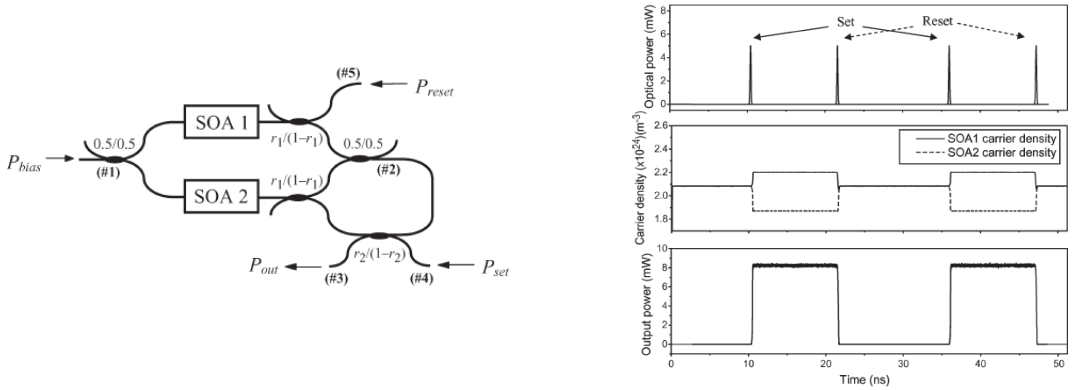

(a) (b)

Fig. 8. (a) Proposed architecture for the chaotic carrier generator based on a single SOA-MZI with optical feedback loop [21]. (b) Example of temporal traces for the flip-flop operation [21].

The above-shown architecture has already been extensively studied in the literature. In particular, it has been demonstrated that bistability can be forced on this sort of configuration [22].

It means that flip-flop operation can be achieved, since two possible stable states which can be dynamically changed by external control pulses may be switched.

The principle of operation as a flip-flop behavior of the presented architecture is as follows. A continuous-wave (CW) optical signal of power P_{bias} is injected into the input port #1 of the SOA-MZI. Both the input and the output couplers provide a phase shift of $\pi/2$ radians between the MZI branches. Therefore, in absence of other input signals, no optical power is obtained at the SOA-MZI output port #2 as a consequence of a destructive interference at the output coupler. The output port #2 is interconnected through a feedback loop to the lower MZI branch by means of an optical coupler. Inside the feedback loop, another coupler is also used for extracting the output signal from the optical flip-flop, port #3, as well as for introducing the set pulses, port #4, which act as enabling signals. Finally, an optical coupler is used in the upper MZI branch to balance the interferometer and to allow the introduction of reset pulses through port #5, which act as disabling signals [21].

When injecting a set pulse into the architecture through the port #4, the carrier density and, therefore, the gain is reduced at the SOA 2. In this way, the interferometric structure becomes unbalanced, and the CW signal experiences different gains and phase shifts along both MZI branches, which gives as a result a certain power level at port #2 (Fig. 8(b)). The main function of the feedback loop is to forward a fraction of the output power in port #2 into the SOA 2 in order to hold its state when the optical power of the set pulse vanishes. The output power of the optical flip-flop and the input energy needed for the set pulses can be set by adjusting the coupling factor which is inside the feedback loop. Conversely, when injecting a reset pulse into port #5, it arrives to SOA 1 and reduces its carrier density and optical gain in a similar way, but due to the feedback loop, the carrier density in SOA 2 is also changed (Fig. 8(b)). If injecting a reset pulse with energy high enough, the flip-flop state is switched. So, the SOA-MZI becomes balanced again, resulting in an output power at port #2 equal to zero [21].

The strength of the feedback loop has important influence on the performance of the architecture and it plays an important role when talking about stability. Specifically, when the strength of the feedback loop becomes significant, it provides an extra dimension to the phase space, fact which strongly modifies the dynamics. Once it is modified in this sense, it can be affected by irregular behavior. Hence, the introduction of high enough feedback strength provides two extra dynamical degrees of freedom, which are sufficient to yield self-pulsing and chaotic behavior when the loop length and coupling factor r_2 are appropriately chosen. Detailed performance results as a function of different system parameters are given in section IV.

III. Analytical model

In section II, the qualitative behavior of the proposed system has been detailed. Now, an analytical description is derived for the purpose of accurately model the dependences of the most important physical parameters on the performance.

III.1. *SOA-MZI-based system with optical feedback.*

The theoretical model reported is based on the approach proposed by Agrawal, which models the propagation of a single optical carrier through a semiconductor waveguide by means of the following set of coupled differential equations [23]. It is assumed by the model that the CW carrier is placed at the SOA peak-gain wavelength. Otherwise, a gain reduction coefficient should be applied.

$$\frac{\partial P(z,\tau)}{\partial z} = [g(z,\tau) - \alpha_{\text{int}}]P(z,\tau) \tag{12}$$

$$\frac{\partial \phi(z,\tau)}{\partial z} = -\frac{1}{2}\alpha_N g(z,\tau) \tag{13}$$

$$\frac{\partial g(z,\tau)}{\partial t} = \frac{g_0(z,\tau) - g(z,\tau)}{\tau_c} - \frac{g(z,\tau)P(z,\tau)}{E_{sat}} \tag{14}$$

Where τ represents the reduced time, which is given by $\tau = t - z / v_g$ with $v_g = c / n_g$, being v_g the group velocity and n_g the group index. According to the definition of the field envelope, which is expressed as $A = [P(z,\tau)]^{1/2}\exp\{j\Phi(z,\tau)\}$, $P(z,\tau)$ and $\Phi(z,\tau)$ are the power and the phase of the optical wave. On the other hand, α_{int}, g, g_0, α_N, τ_c and E_{sat} are the internal loss, the gain, the small-signal gain, the linewidth enhancement factor, the carrier lifetime and the saturation energy respectively.

$$g(z,\tau) = \Gamma a(N - N_0) \tag{15}$$

$$g_0(z,\tau) = \Gamma a\left(\frac{I\tau_c}{qV} - N_0\right) \tag{16}$$

$$E_{sat} = h\upsilon\frac{\omega d}{\Gamma a} \tag{17}$$

$$\tau_c = \frac{1}{A + BN + CN^2} \tag{18}$$

Being Γ the confinement factor, a the differential gain, I the injection current, q the electron charge, V the active cavity volume, N the carrier density, N_0 the carrier density at transparency, $h\upsilon$ the photon energy, and ωd the cross-section of the active layer. A, B and C are the linear recombination, the bimolecular recombination and the Auger recombination coefficients respectively.

A numerical method is required in order to solve the coupled differential equation system specified by (12)−(14). Nevertheless, if the assumption $\alpha_{int} << g$ is taken into account, the previous equations can be simplified considerably. This condition is often satisfied in practice [21]. Hence, by integrating (12) and (13) over the active cavity length, the output power and the output phase can be expressed as a function of the input slow-varying field envelope as:

$$P(z=L,\tau)=P(z=0,\tau)e^{h(\tau)} \tag{19}$$

$$\phi(z=L,\tau)=\phi(z=0,\tau)-\frac{1}{2}\alpha_N h(\tau) \tag{20}$$

being L the active cavity length and $h(\tau)$ the gain transfer function of the SOA, which is mathematically defined as:

$$h(\tau)=\int_{z=0}^{z=L} g(z,\tau)dz \tag{21}$$

By making use of the above-mentioned transfer function, the so-called *instantaneous amplifier gain* can be calculated as $G(\tau)=exp\{h(\tau)\}$ [21]. Finally, via integrating equation (14) over the active layer length and taking in consideration the result derived from (19), $h(\tau)$ can be found as the solutions of the following nonlinear differential system made up by two equations, one for each SOA [21].

$$\frac{\partial h_i(\tau)}{\partial \tau}=\frac{g_0 L-h_i(\tau)}{\tau_c}-\frac{P_{in,SOA_i}}{E_{sat}}\left[e^{h_i(\tau)}-1\right] \tag{22}$$

Where i refers to the ith SOA, being i = 1, 2. The term $P_{in,SOAi}$ stands for the total optical power entering SOA_i which is comprised of different contributions as shown in Fig. 8(a). By carrying out a detailed analysis of the propagation of the different contributions existing in each point of the structure, the total input power for both amplifiers can be obtained as [21]:

$$P_{in,SOA_1}=r_1P_{reset}+\frac{1}{2}P_{bias}+\frac{1}{4}r_1(1-r_1)(1-r_2)P_{bias}e^{\overline{h_2}} \tag{23}$$

$$P_{in,SOA_2}=r_1r_2P_{set}+\frac{1}{2}P_{bias}+r_1(1-r_1)(1-r_2)P_{bias}\left[e^{\overline{h_2}}+\frac{1}{4}e^{\overline{h_1}}-\sqrt{e^{\overline{h_1}}\cdot e^{\overline{h_2}}}\cos\left\{\frac{1}{2}\alpha_N\left(\overline{h_1}-\overline{h_2}\right)\right\}\right] \tag{24}$$

where $\overline{h_i}$ is the delayed version of h_i due to the feedback loop. By defining τ_0 as the feedback-loop delay, the delayed version can be written as follows [21].

$$\overline{h_i}(\tau)=h_i(\tau-\tau_0) \tag{25}$$

III.2. *Stability analysis.*

Equations (22)−(24) makes up a non-linear non-autonomous differential equation system, which must be numerically solved in order to obtain the transfer function of each SOA embedded in both branches of the interferometric structure. Performing stability analysis of the structure is of great importance to clearly distinguish between stable and unstable regions.

In order to route the structure to chaos, nonlinear behavior must be forced on the semiconductor waveguides for the purpose of generating complex dynamics. Furthermore, the strength of the feedback loop must be also carefully set by controlling the length and the coupling factor, which adjusts the amount of the output power re-injected again into SOA 2. In the table below, the values taken into account for the simulations carried out in this work are depicted. Some of them have been kept constant during the simulation framework, whereas the values of other specific ones have been varied for the purpose of studying their impact on the structure behavior.

Symbol	Parameter description	Value
L	SOA length	500 μm
ωd	Transversal section	$2 \cdot 10^{-13}$ m^2
V	Active cavity volume	$1 \cdot 10^{-16}$ m^3
a	Differential gain	$3 \cdot 10^{-20}$ m^2
N_0	Carrier density at transparency	$1.5 \cdot 10^{24}$ m^{-3}
V	Active cavity volume	$1 \cdot 10^{-16}$ m^3
Γ	Confinement factor	0.4
n_g	Group index	3.4
α_N	Linewidth enhancement factor	8
I_{SOA1}	Bias current	600 mA
I_{SOA2}	Bias current	600 mA
P_{bias}	CW input optical power	2 mW
λ_0	Nominal wavelength	1550 nm
r_1	Coupling factor	0.5
r_2	Coupling factor	0.7
τ_0	Feedback-loop delay	300 ps
A	Linear recombination coefficient	$0.5 \cdot 10^{8}$ s^{-1}
B	Bimolecular recombination coefficient	$5 \cdot 10^{-16}$ m^{3}s^{-1}
C	Auger recombination coefficient	$5 \cdot 10^{-41}$ m^{6}s^{-1}

Table 1: Setting parameters of the proposed system [21]

III.2.1 *Static behavior.*

As a first resort, the steady-state solution of the nonlinear delay differential system made up by equations (22)−(24) is obtained. For this purpose, some important considerations have to be taken into account, which concern the dynamics, the feedback-loop delay, and the input powers of the set and reset pulses.

$$\frac{\partial h_i(\tau)}{\partial \tau} = 0, \quad i = 1,2 \tag{26}$$

$$P_{set} = P_{reset} = 0 \tag{27}$$

$$\overline{h_i}(\tau) = h_i(\tau), \quad \tau_0 = 0 \tag{28}$$

By modifying equations (22)−(24) according to (26)−(28), the stability theory of autonomous systems may be applied [24]. If plotting the results obtained in maps of the form h_1 versus h_2, the crossovers between both traces set the steady-state solutions or fixed points. Via using the setting parameters depicted in table 1, 5 fixed points characterizes the dynamics of the system. The couple of values $(h_1, h_2)_j$, with $j \in [1,5]$, satisfies the rate equation (22) for SOA 1 and SOA 2 simultaneously.

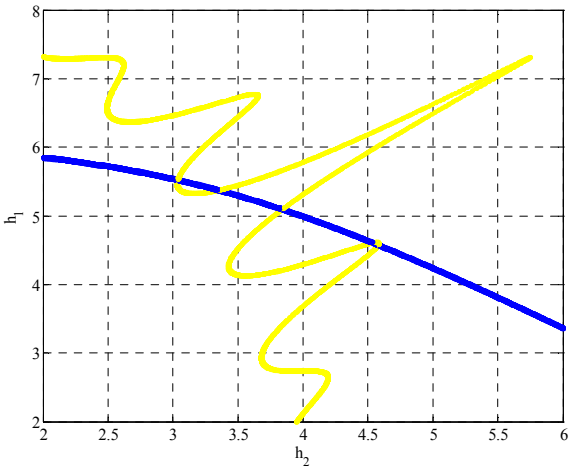

$(h_1, h_2)_1 = (5.5166, 3.0284)$

$(h_1, h_2)_2 = (5.3702, 3.3397)$

$(h_1, h_2)_3 = (5.0911, 3.8313)$

$(h_1, h_2)_4 = (4.6023, 4.5307)$

$(h_1, h_2)_5 = (4.5712, 4.5712)$

Fig. 9. Steady-state curves for both SOAs. Blue trace refers to SOA 1 solution and the yellow one to SOA 2 solution. Intersections between both establish the fixed points.

Once calculated the value of all the five steady-state solutions, a stability study must be carried out for taking aim at deciding if stable or unstable behavior occurs. In order to determine the stability of a fixed point, the Jacobian matrix of (22) needs to be evaluated [24].

$$J_j = \left[\begin{array}{cc} \frac{\partial}{\partial h_1}\left\{\frac{dh_1}{d\tau}\right\} & \frac{\partial}{\partial h_2}\left\{\frac{dh_1}{d\tau}\right\} \\ \frac{\partial}{\partial h_1}\left\{\frac{dh_2}{d\tau}\right\} & \frac{\partial}{\partial h_2}\left\{\frac{dh_2}{d\tau}\right\} \end{array} \right]_{(h_1,h_2)_j} \tag{29}$$

According to the stability theory [24], a fixed point $(h_1, h_2)_j$ is found to be stable if all the eigenvalues of its J_j matrix are characterized by a negative real part. In this manner, the characteristic equation must be solved for the purpose of obtain the corresponding eigenvalues.

$$\det\left(\lambda_j I - J_j\right) = 0 \tag{30}$$

Where here I refers to the identity matrix, $det(\cdot)$ is the determinant, and λ_j are the eigenvalues of the matrix J_j. By calculating the eigenvalues when considering each fixed point, one can determine their stability, which can be summarized as follows.

Real part of the eigenvalues	Stability
$Re\{(\lambda_1, \lambda_2)_1\} = (-2.32\cdot10^{11}, -4.67\cdot10^{11})$	Stable
$Re\{(\lambda_1, \lambda_2)_2\} = (-3.29\cdot10^{11}, 4.03\cdot10^{11})$	Unstable
$Re\{(\lambda_1, \lambda_2)_3\} = (-0.33\cdot10^{12}, -1.23\cdot10^{12})$	Stable
$Re\{(\lambda_1, \lambda_2)_4\} = (-3.72\cdot10^{11}, 3.51\cdot10^{11})$	Unstable
$Re\{(\lambda_1, \lambda_2)_5\} = (-3.73\cdot10^{11}, -3.73\cdot10^{11})$	Stable

Table 2: Stability results of the different fixed points

In accordance with the nonlinear systems' theory [25], and by making use of a geometric way of thinking, conclusions regarding the stability of a fixed point may be also derived by studying the sign of the flow's slope in the certain point. By taking as a reference trace the solution for the SOA 1, if the derivative of the solution for the SOA 2 becomes positive, then the fixed point presents repelling nature and therefore is an unstable point. On the other hand, when presenting attracting nature due to a negative slope, the fixed point is stable. There is another way to discern if a fixed point meets the stability condition, which is based on the physical idea of the potential energy. Specifically, local minima of the potential energy of the system correspond to stable fixed points, whereas local maxima to unstable ones [25].

Finally, by keeping in mind the proposed architecture shown in Fig. 8(a), the output power P_{out} as a function of the transfer function of both SOAs under the conditions expressed in (26)−(28), as well as the different system parameters can be written as [21]:

$$P_{out}(\tau) = \frac{1}{2} P_{bias}(1 - r_1) r_2 \left[\frac{e^{h_1(\tau)} + e^{h_2(\tau)}}{2} - \sqrt{e^{h_1(\tau)} e^{h_2(\tau)}} \cos\left(\frac{1}{2} \alpha_N \left(h_1(\tau) - h_2(\tau) \right) \right) \right] \tag{31}$$

It becomes interesting to notice that a null output power is obtained when considering the condition $h_1 = h_2$, which corresponds to the fixed point number five.

III.2.2 *Dynamic behavior.*

Once gained knowledge of the quantitative behavior of the proposed system under static conditions (26)−(28), it is time to study the structure when supposing dynamic effects, such as transients and the response to input stimuli (set and reset pulses). For this purpose, it must be highlighted that (22)−(24) turns into a nonautonomous system of functional differential equations, since $\tau_0 \neq 0$. Fortunately, it falls into the category of delay differential equations system with constant delays, which have been extensively studied.

Keeping in mind that the structure is found to be used as a chaotic carrier generator, it is not so much interesting to study the response of the structure under the injection of input stimuli. The reason is that it is not necessary to change the dynamics between different working points, just set one and provide routing to chaotic behavior by controlling certain system parameters.

By the fact of considering nonzero delay time of the feedback loop, the characteristic equation which must to be solved, according to the stability theory becomes [24]:

$$\det\left(\lambda_j I - J_j^{(0)} - J_j^{(1)} e^{-\lambda_j \tau_0}\right) = 0 \tag{32}$$

where the matrices $J^{(0)}$ and $J^{(1)}$ are the Jacobian with $h_i(\tau)$ and $h_i(\tau-\tau_0)$ respectively. As before, those matrices have to be evaluated at the different fixed points in order to obtain their stability. Taking into account that $(h_1(\tau), h_2(\tau))_j = (h_1(\tau-\tau_0), h_2(\tau-\tau_0))_j$, so:

$$J_j^{(0)} = \left[\begin{array}{cc} \frac{\partial}{\partial h_1}\left\{\frac{dh_1}{d\tau}\right\} & \frac{\partial}{\partial h_2}\left\{\frac{dh_1}{d\tau}\right\} \\ \frac{\partial}{\partial h_1}\left\{\frac{dh_2}{d\tau}\right\} & \frac{\partial}{\partial h_2}\left\{\frac{dh_2}{d\tau}\right\} \end{array}\right]_{(h_1,h_2)_j} \qquad J_j^{(1)} = \left[\begin{array}{cc} \frac{\partial}{\partial \overline{h_1}}\left\{\frac{dh_1}{d\tau}\right\} & \frac{\partial}{\partial \overline{h_2}}\left\{\frac{dh_1}{d\tau}\right\} \\ \frac{\partial}{\partial \overline{h_1}}\left\{\frac{dh_2}{d\tau}\right\} & \frac{\partial}{\partial \overline{h_2}}\left\{\frac{dh_2}{d\tau}\right\} \end{array}\right]_{(h_1,h_2)_j} \tag{33}$$

The roots of (32) are known as characteristic roots and determine the local stability of the fixed point. Negative real part of all the eigenvalues stands for stable behavior, whereas it is unstable if there is any root characterized by positive real part. It is important to mention that a Hopf bifurcation occurs when the real part of a pair of complex conjugate characteristics roots becomes positive. If the system undergoes a Hopf bifurcation, the stable fixed point changes its dynamics to a limit cycle [21].

IV. Numerical results

In the present section, numerical calculations of the degree of chaos reached by the proposed system under certain initial conditions are depicted. With the goal of accounting for how chaotic the structure is, the value of the *Global Lyapunov Exponent (GLE)* is obtained as a function of the most important controlling parameters. The GLE is calculated by making use of a neural network-based algorithm which meets the Jacobian approach [12]. Just mention that, although noise considerations have been skipped over in the simulation process, the Jacobian approach has been implemented in order to allow possible future numerical calculations of noisy systems.

Studies carried out in the present work have shown that the variables $h_1(\tau)$ and $h_2(\tau)$ become chaotic when setting the appropriate values of certain parameters, as well as when the proper initial conditions are accurately chosen. It means that at the output of each SOA, chaotic behavior can be achieved independently. According to the architecture of the proposed system (see Fig. 8(a)), the output power is taken from somewhere inside the feedback loop. Because of the interferometric phenomenon that takes place at the output coupler of the Mach-Zenhder structure, both contributions coming from both arms are combined. Although identical SOAs are considered, which are also biased with the same current level, the output power of both SOAs differs in their amplitude. This fact is caused by the different gain which experiences the optical carrier along both arms due to the power excess injected into SOA 2 by the feedback loop. Moreover, the output power of the SOA 2 at a given reduced time τ is also function of the power which was at the output of the interferometric structure τ_0 seconds before. Taking into account the above-mentioned considerations, as a result of combining both optical carriers passing through both arms, the total power tested at port #3 brakes the aperiodicity which characterizes both SOAs outputs. Owing to the appearing of periodic components in the total power, to the best of our knowledge, it is not possible to route it to chaotic behavior.

In order to overcome this limitation, the tests have been performed by considering the optical signal provided by port #5. In this way, the sort of correlation between both transfer functions at the interferometric output port has not important repercussions on the new output power. Hence, from now on, port #5 will be referred as the output port, and its output power can be defined as follows by keeping in mind the static conditions expressed in (26)−(28).

$$P_{out}(\tau) = \frac{1}{2} P_{bias} r_1 e^{h_1(\tau)} \tag{34}$$

On one hand, the impact of the strength of the feedback loop on the nature of the system's behavior has been characterized. The study has been carried out in terms of the feedback loop delay and the coupling factor r_2, which defines the amount of power re-injected into the SOA 2 by the loop.

On the other hand, the effect produced by the SOA dynamics on the system's behavior has also been object of study. Specifically, numerical calculations have been performed as a function of the injection currents and the input power.

In all the simulations performed, data arrays of 30001 points have been used as inputs of the algorithm for calculating the GLE. It must be highlighted that the transients of the solutions have not been considered for creating the data arrays; it means that only steady-state points are taken into account. In order to design the neural network used for approximating the points given by a certain input data array, 3 dimension parameters must be defined. The triplet *(L, m, q)* defines the complexity of the chaotic map. Theoretically, as the values of these parameters increase, the neural net function (which must be also defined) can approximate any smooth, nonlinear function to arbitrary accuracy. However, over-dimensioned neural networks will give as a result a run-time excess. The optimum solution consists of dynamically adjusting the dimensionality of the neural network according to the dynamics complexity. Nevertheless, this solution requires an in-depth study of the output signal. For simplicity purposes, the triplet *(L, m, q)* has been fixed to *(7, 8, 7),* which is good enough for providing accurate results over all the cases under study. The mean run-time of the algorithm by taking into account data arrays of 30001 points and the above-defined dimensionality is approximately 20 hours. The starting point, which defines the initial condition for running the algorithm, has been set to $h_1(\tau=0)=3.96$ and $h_2(\tau=0)= 3.61$ for all the simulations performed.

IV.1 *Chaotic behavior as a function of the feedback loop delay.*

To study the effect of the feedback loop length on the dynamics of the system, the behavior of the output power when sweeping the loop delay τ_0 is characterized.

With the goal of demonstrating that chaotic behavior occurs under certain loop delays, the GLE is calculated considering different scenarios. Moreover, the time traces, the spectra and the phase spaces are also subject of study because they can be useful indicators of chaos.

It must be noticed that the degrees of freedom of the set of equations which model the system, consists of $h_1(\tau)$, $h_2(\tau)$, and their corresponding delayed versions, $h_1(\tau-\tau_0)$ and $h_2(\tau-\tau_0)$. Therefore, the embedding dimension of the system is 4. It means that to gain full geometrical information from the nature of the attractor in the phase space, four-dimensional plots should be calculated. Since the phase space results shown are two-dimensional, information in two directions is only given. However, interesting practical conclusions can be derived.

Fig. 10 depicts the numerical calculations of the GLE as a function of the loop delay, which has been varied from 10 to 500 ps. All the system parameters are set to the values specified by Table 1, unless for the loop delay τ_0.

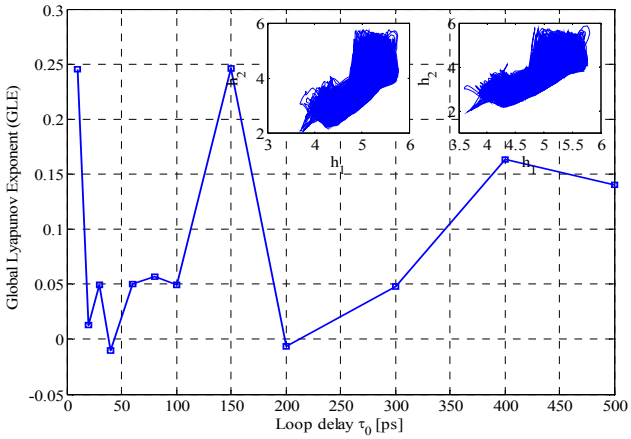

Fig. 10. GLE as a function of the feedback loop delay τ_0. The insets show the attractor in the phase space when $\tau_0 = 40$ *ps* (left-hand) and when $\tau_0 = 150$ *ps* (right-hand).

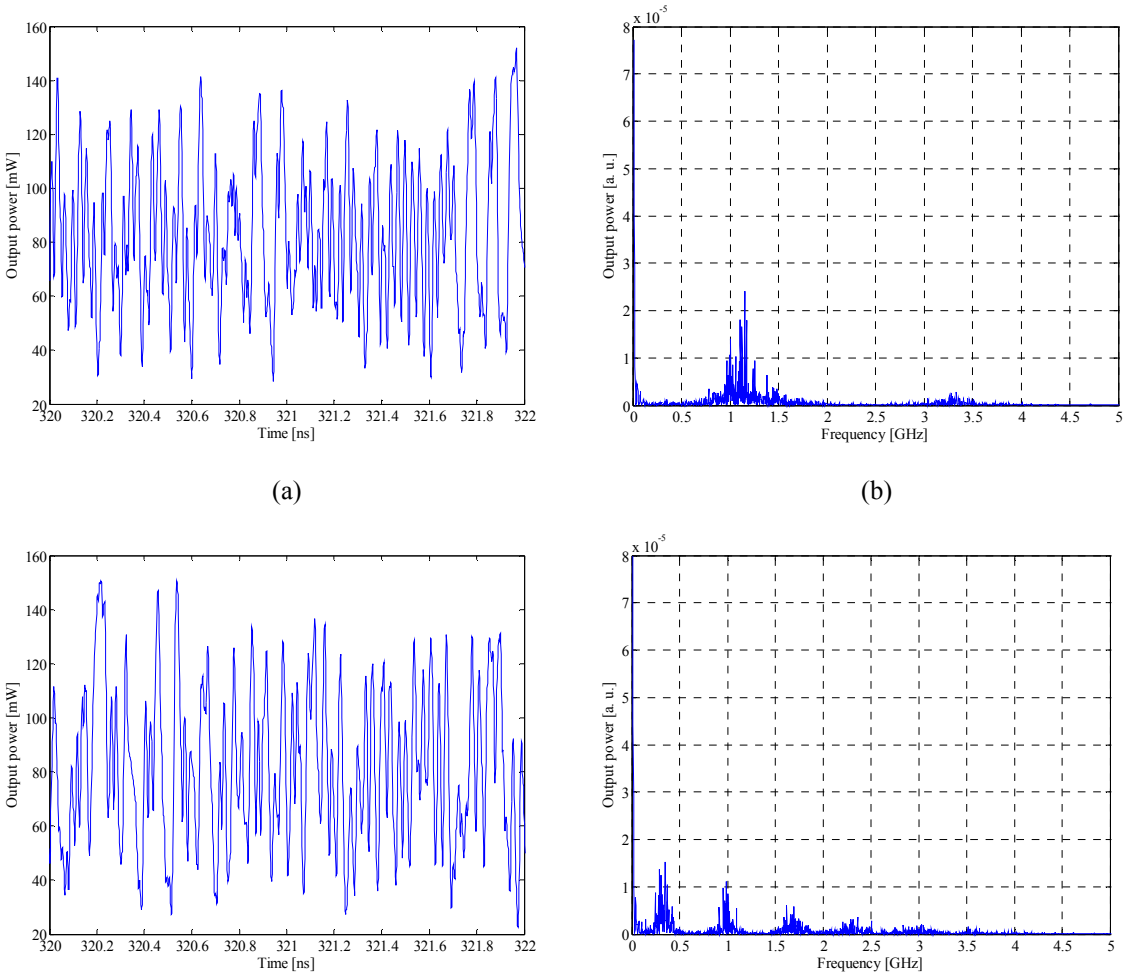

Fig. 11. (a) Time trace when $\tau_0 = 40$ *ps*. (b) Spectrum when $\tau_0 = 40$ *ps.* (c) Time trace when $\tau_0 = 150$ *ps*. (d) Spectrum when $\tau_0 = 150$ *ps.*

As one can see, by the fact of connecting the feedback loop, the structure reports chaotic behavior whatever the delay. The only points characterized for high enough periodic components able to break the aperiodicity are $\tau_0 = 40\ ps$ and $\tau_0 = 200\ ps$. The GLE for these values of the loop delay are slightly below than zero. In these cases, it is far from straightforward to discern periodic components from aperiodic ones in the phase spaces. The reason is because the structure becomes stable after a long time, so the aperiodic behavior is superimposed to the periodic one. That is the reason why the phase space seems to present strange behavior (see the left-hand inset in Fig. 10), but certainly is periodic, as the sign of the GLE indicates. Therefore, from visual inspection of the phase spaces, conclusions cannot be appropriately drawn. The right-hand inset in Fig. 10 shows the nature of the phase space when setting $\tau_0 = 150\ ps$. According to its GLE, for this delay the maximum strangeness output is obtained.

On the other hand, the time traces at the output port and their corresponding spectra are shown in Fig. 11. Chaotic signals are characterized by strange behavior, fact which is in good agreement with the totally aperiodic waveform and the flat spectrum shown in (c) and (d) respectively. However, periodicity appears in (a) and (b), since the waveform and the spectrum discern strong enough periodic components for reporting a negative GLE.

IV.2 *Chaotic behavior as a function of the feedback loop strength.*

In order to carry out a complete characterization of the impact of the feedback loop on the performance of the system, numerical calculations involving the amount of power re-injected into SOA 2 are accomplished.

For this purpose, the coupling factor r_2 has been swept from 0, i.e., when no feedback loop is taken into account, to 0.9, where the 90% of the power existing at port #2 is feedback into SOA 2. As before, the study is fulfilled in terms of the GLE, as well as the time traces, the optical spectrum, and the phase space.

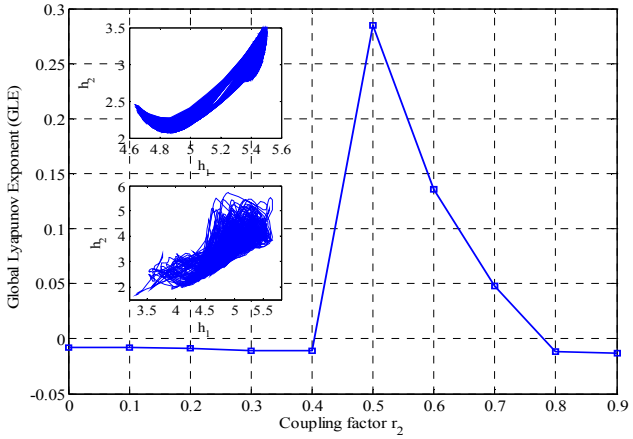

Fig. 12. GLE as a function of the coupling factor r_2. The insets show the attractor in the phase space when $r_2=0.2$ (upper) and when $r_2=0.5$ (lower).

In figure above, the evolution of the GLE as a function of the coupling factor is shown. All the system parameters are set to the values specified by Table 1, unless for the coupling factor r_2. As one can see, the chaotic behavior is reached by the structure when adjusting the coupling factor between 0.41 and 0.78 approximately. Moreover, the optimum value of the coupling factor which generates the most chaotic dynamics at the structure's output is 0.5. On the other hand, the insets refer to the phase space when considering specific cases. The upper inset depicts the phase space nature when setting the coupling factor $r_2 = 0.2$. As it is shown, the attractor in the phase space consists of a sort of limit cycle; which is disturbed because apart from the most significant periodic perturbation, there also exist other spectral components characterized by lower amplitude. The lower inset stands for the phase space when considering $r_2 = 0.5$. It is a clear example of a strange attractor, in which the dynamics seems to follow a totally aperiodic behavior.

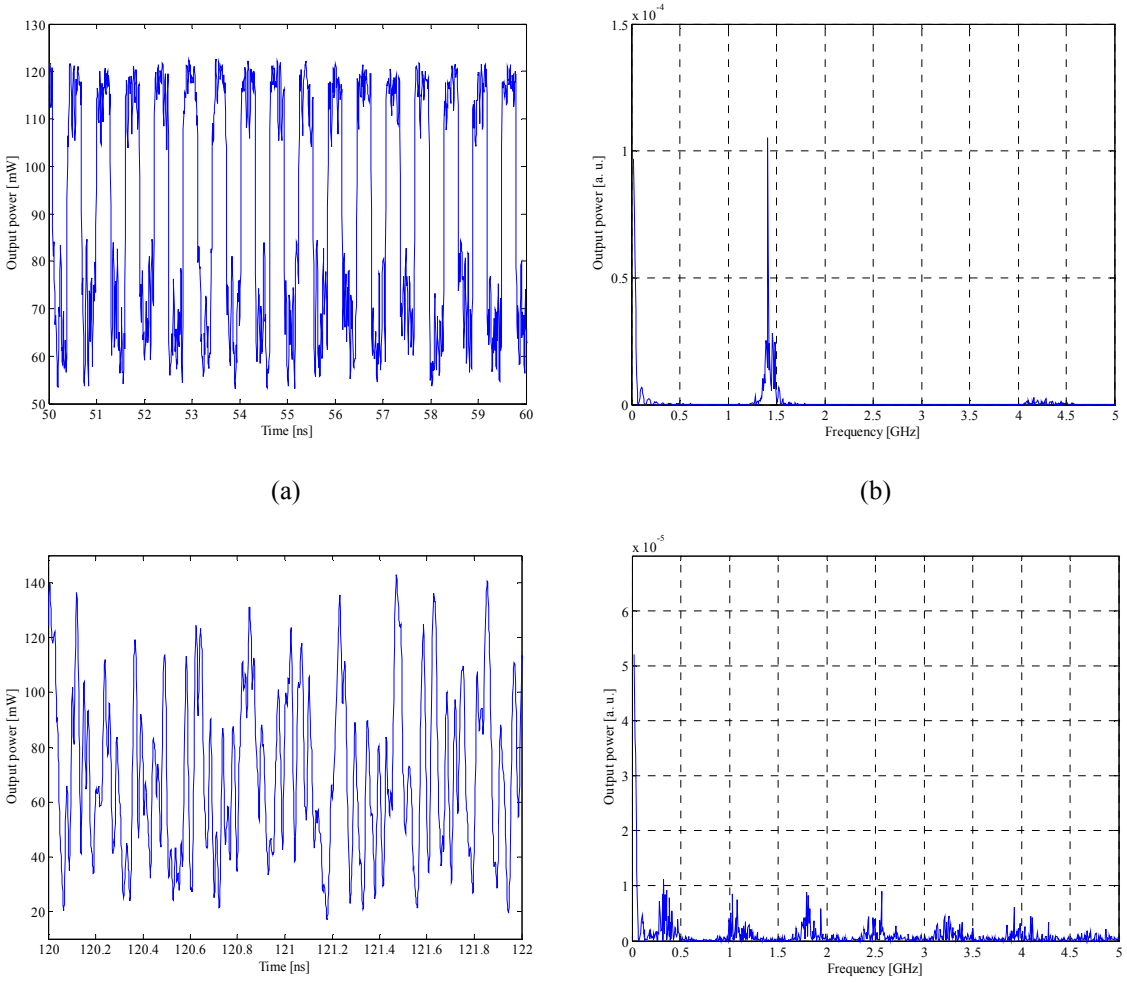

Fig. 13. (a) Time trace when $r_2=0.2$. (b) Spectrum when $r_2=0.2$. (c) Time trace when $r_2=0.5$. (d) Spectrum when $r_2=0.5$.

Fig. 13 summarizes the time traces and the spectra of the system's output when the coupling factor is set to 0.2 and 0.5 respectively. In Fig. 13(a), clear periodic behavior can be observed, fact

which is perfectly consistent with the results drawn from the phase space. It must be noticed that on the maxima and minima of the periodic perturbation, a sort of ripple is superimposed. That is the reason why the attractor is disturbed from the typical appearance of a limit cycle. If attention is paid on the spectral characterization (Fig. 13(b)), one can clearly see the line representing the periodic perturbation, as well as other contributions with lower amplitude due to the above-mentioned ripple. Fig. 13(c) shows the time trace when the attractor becomes strange. Apparently the trace does not follow any periodic pattern, since periodic components cannot be discerned. This fact agrees the spectral characterization because it is roughly flat (Fig. 13(d)).

IV.3 *Chaotic behavior as a function of the injection currents.*

The impact of the feedback loop on the nature of the output power has been characterized in terms of its delay and strength in the last sections. Now, the dependence of the SOA dynamics on the degree of chaos reached by the structure is deeply studied. The controlling parameters used for adjusting the dynamics generated by both SOAs are the injection currents and the input powers.

Firstly, the GLE is calculated as a function of the current injected into the SOAs. Both the amplifiers are biased with the same current level, which has been swept from 100 mA to 800 mA. As one can see in Fig. 14, the structure generates chaotic behavior over a wide range of injection currents. However, when considering injection currents between 290 mA and 420 mA approximately, the GLE becomes negative giving as a result non-chaotic behavior. This fact is caused by a change in the stability of the structure. Probably, as a result of a bifurcation, the structure becomes stable due to the appearing of periodic components. In this case, it is not easy to discern periodic components from aperiodic contributions in the phase spaces. The reason is because the structure becomes stable after a long time, so the aperiodic behavior is superimposed to the periodic one. Therefore, from visual inspection of the phase spaces, conclusions cannot be appropriately derived.

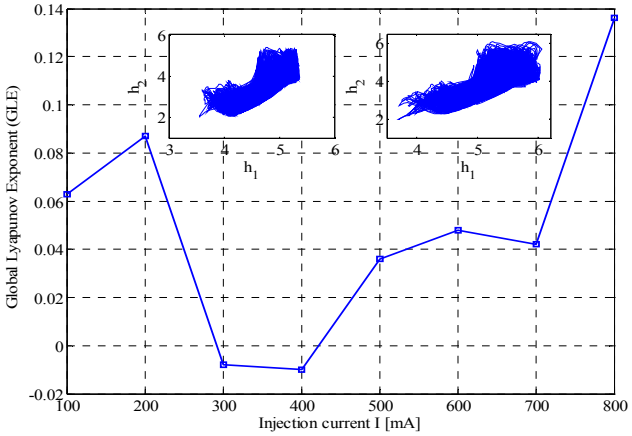

Fig. 14. GLE as a function of the injection currents *I* into both SOAs. The insets show the attractor in the phase space when *I=400 mA* (left-hand) and when *I=800 mA* (right-hand).

The corresponding time traces and spectra for both currents under study are presented in Fig 15. These indicators of chaos provide more useful information than the phase space. From the spectra shown in (b) and (d), one can assure that both contain periodic components. However, when setting the highest current, more harmonics can be discerned in the spectral characterization, but with roughly the same power level. In this sense, the spectrum approaches to a flatter spectrum more than the case of biasing with *I = 400 mA*. Flat spectra are typical of chaotic signals. From the time traces (a) and (c) becomes difficult to discern the strange behavior from the case in which non-chaotic output is obtained.

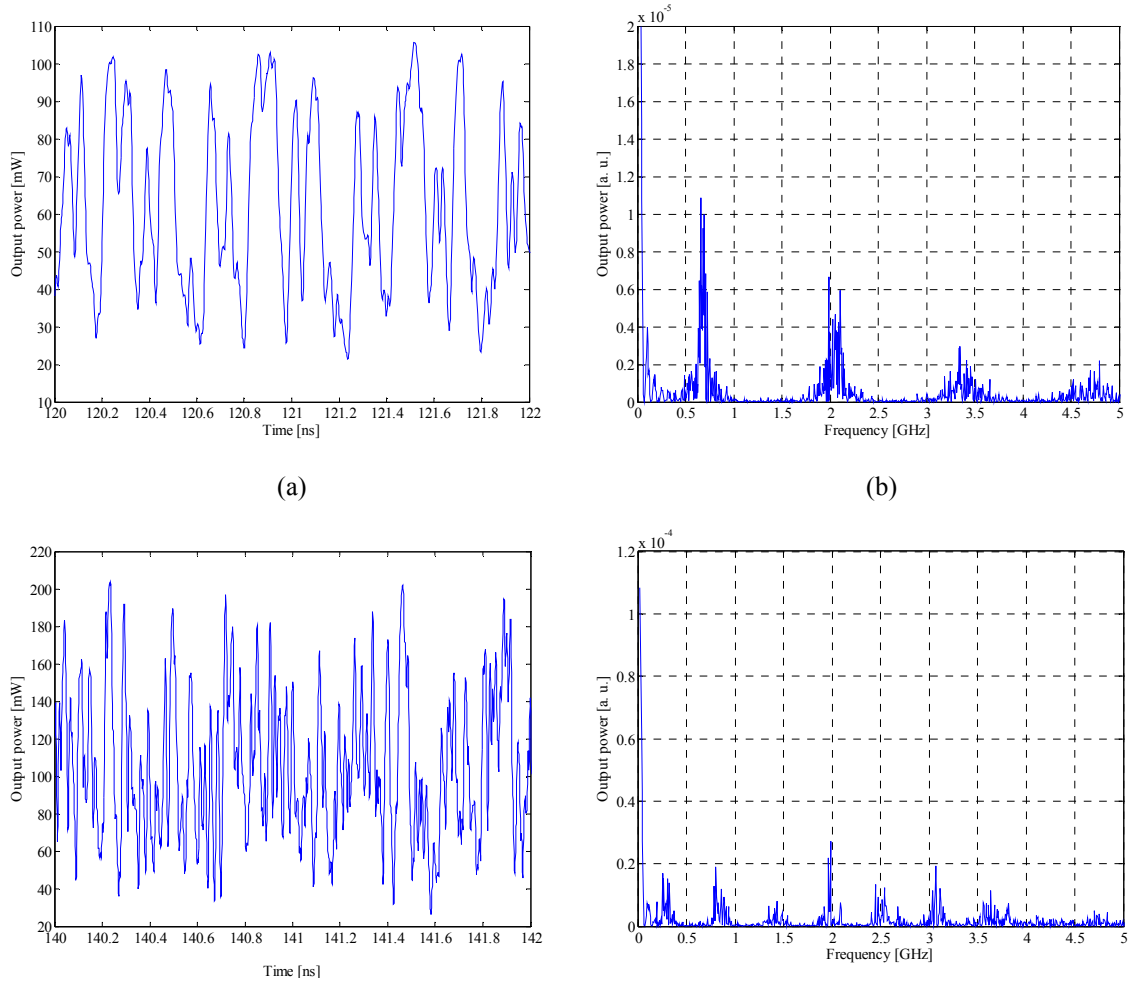

Fig. 15. (a) Time trace when *I = 400 mA*. (b) Spectrum when *I = 400 mA*. (c) Time trace when *I = 800 mA*. (d) Spectrum when *I = 800 mA*.

IV.4 *Chaotic behavior as a function of the input power.*

Finally, the chaotic behavior is studied as a function of the input power. It must be mentioned that the input power refers to the power injected into the port #1 of the structure P_{bias} (see Fig. 8(a)). Therefore, the power injected into each SOA is a halved due to the input coupler.

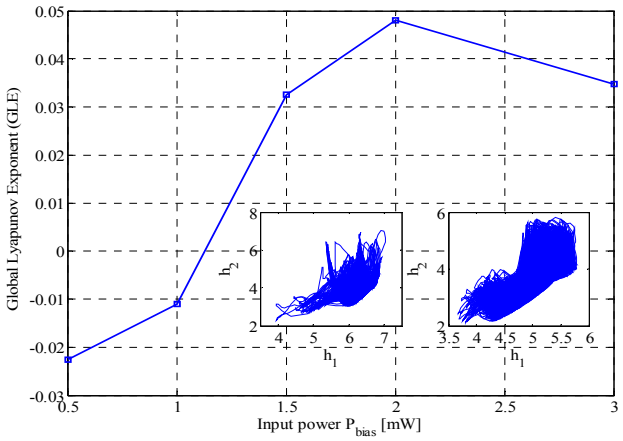

Fig. 16. GLE as a function of the input power P_{bias}. The insets show the attractor in the phase space when $P_{bias} = 0.5\ mW$ (left-hand) and when $P_{bias} = 2\ mW$ (right-hand).

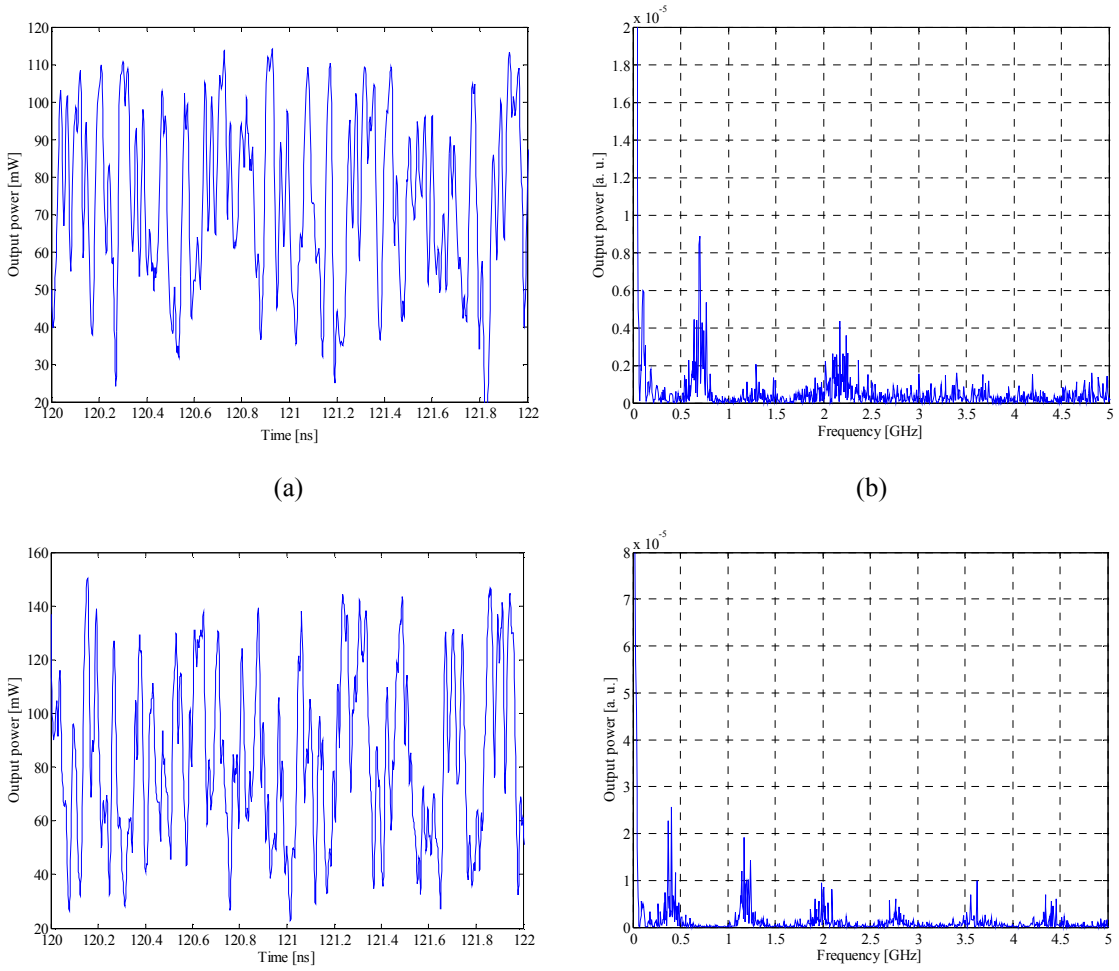

(a) (b)

(c) (d)

Fig. 17. (a) Time trace when $P_{bias} = 0.5\ mW$. (b) Spectrum when $P_{bias} = 0.5\ mW$. (c) Time trace when $P_{bias} = 2\ mW$. (d) Spectrum when $P_{bias} = 2\ mW$.

Loosely speaking, the larger the input power, the higher the GLE will be (see Fig. 16). The threshold value of the input power for guaranteeing chaotic behavior is approximately 1.25 mW, when considering the values of the parameters summarized in Table 1. However, for larger bias powers, the value of the GLE suffers saturation.

It means that the degree of chaos increases with the input power, because more complex dynamics are achieved at the output of the structure. The reasoning is as follows. If good enough bias power is applied at the input of a semiconductor device, the gain saturation effect will take place. The aforementioned effect gives as a result a non-linear gain response and, therefore, complex dynamics. The left-hand inset depicts how the attractor in the phase space follows a pseudo-periodic pattern. Specifically, the shape of the attractor approaches a sort of disturbed saddle function. In this sense, the attractor is somewhat predictable. On the other hand, the right-hand inset shows the attractor when injecting an input power of 2 mW. It seems to be strange since as far as one can discern, only non-periodic contributions appear.

In this case, from the time traces become difficult to assure if the structure has been routed or not to chaotic behavior (Fig. 17(a)-(c)). However, when low input power is applied, the spectrum is characterized by 2 predominant periodic components (Fig. 17(b)). For larger input powers, the spectrum displays several periodic contributions generated by the nonlinear gain response. Nevertheless, their amplitude is not found to be enough for forcing negative GLE.

V. Conclusions and further work

A novel all-optical structure based on a single SOA-MZI with optical feedback loop has been presented for the purpose of implementing chaotic carrier generation functionalities. Up until now, bistability behavior has already been demonstrated by this kind of structure in the literature. However, as far as we concern, it is demonstrated for the first time in the present work that the structure can be routed to chaotic behavior under certain initial conditions.

The main application of chaos is found to be the implementation of secure communications in optical data networks. Chaos-based security does not focus on competing with quantum cryptography or software encryption, but it has arisen as an efficient solution to complement them. The reason why chaos has become attractive for researchers is because it represents a fully all-optical hardware-based solution, which can be directly implemented on the physical layer. It must be highlighted that implement functionalities directly on the physical layer reports a non negligible series of advantages with respect to implement them on the electrical domain, which must not be overlooked.

Analytical and numerical investigations have been carried out with the goal of accurately modeling the behavior of the proposed architecture. On one hand, a complete analytical model has been developed in order to obtain proper mathematical description of the behavior of the structure. Following, a deeper insight into the stability properties has been performed, identifying both the stable and unstable fixed points. Finally, a generic neural network-based algorithm which meets the Jacobian approach has been implemented for the purpose of calculating the GLE. The calculus of the aforementioned exponent is pretty enough to decide if the system is chaotic or not, as well as how chaotic it is. As inputs of the numerical algorithm, only is needed to specify the vector containing the data to be evaluated and the dimensionality of the neural network. The dimensionality is directly contingent on the precision of the algorithm. Specifically, the higher the dimensionality, the more accurate results are obtained, because better approximations are performed. However, the run-time is considerably increased when setting higher dimensionality, so special care needs to be taken at the time of adjusting the parameters of the neural network.

By making use of the developed algorithm, calculations of the GLE have been carried out with the aim at characterizing the chaotic behavior of the structure. The numerical results show how chaos can be reached by the structure as a function of the most important controllable parameters. Specifically, the regions in which chaos is present at the structure output are calculated as a function of the loop delay, the loop strength, the injection currents, and the input optical power. These parameters cover the characterization attending to loop properties and to the dynamics generated by the semiconductor waveguides.

Regarding further possible work on this issue, some interesting suggestions are reported below:

- The dimensionality of the neural network has to be dynamically adjusted by accurately setting the optimum combination in each case. In this work, the values of the setting parameters have been over-dimensioned to assure always right computation, and they have been kept fixed for all the cases under study. Take special care of this issue, can provide considerably faster computation.
- To pursue deeper characterization of the GLE as a function of the most important physical parameters of the structure. It must be also taken into account other relevant system parameters that have not been studied in this work, like for instance, the coupling factor r_1.
- To study the response of the structure to input stimuli, it means, when reset and set pulses are injected. Consider the possibility of using these pulses as enabling signals for routing the structure to chaotic behavior instead of changing the value of the controllable parameters.
- To implement the complete transmitter, as well as to evaluate the different modulating schemes for the purpose of choosing that which reports the best performance.
- To implement the complete receiver attending to the open and the close loop designs. In consistency with the performance reported, to choose the best solution.
- Once designed both the transmitter and the receiver, the entire chaos-based communications system must be evaluated. Special careful must be taken into account when implementing the synchronization issues.
- To study the impact of possible mismatch tolerances between some of the most important physical parameters of the chaotic carrier generator of the transmitter and the receiver on the final performance of the system.
- To check out the effect produced on the final performance the fact of linking the transmitter and the receiver by means of an optical fiber. The study should be made, at least, in terms of attenuation and dispersion. Possible nonlinearities generated in the optical link, as well as the assumption of multi-mode fibers (MMF) could be interesting aspects to be also considered.

ACKNOWLEDGEMENTS

The author would like to acknowledge the support given by the European Union within the FP7 project GOSPEL, the Generalitat Valenciana PROMETEO 2008-092 Microwave Photonics Excellency Project, and Plan Nacional I+D TEC2007-68065-C03-01.

I would like to express my warmest gratitude to my supervisor, professor Paco Ramos. He is an inexhaustible fountain of ideas and his advices and valuable guidance have always helped me to keep my work in the right way. I am very proud of working shoulder to shoulder with him, and it would be a pleasure to follow such a nice collaboration for many years.

I am also deeply grateful to professor Salva Sales, who has started me in this nice, but at the same time complex world, giving me the choice to take part in his research group. Thanks a lot for believing in me.

The whole staff of the research group is thanked for creating an ideal job atmosphere, but especially my GOSPEL project mates, because they are the best colleagues that one could wish for.

Finalment, m'agradaria aprofitar aquesta ocasió tan especial per a agrair als meus pares i germans tot el suport que m'han mostrat en totes les etapes de la meua vida. Han segut un pilar fonamental sobre el que m'he recolzat, sense el qual res hagués segut possible. Moltes gràcies a tots. No vull oblidar dedicar aquesta tesina a una persona que ha segut molt especial per a mi, que ara ja fa un any que no gaudis de la seua alegria. Per desgracia, ja mai podrà veure-la acabada, encara que estic segur que estaria orgullosa de mi.

REFERENCES

[1] E. N. Lorentz, *Deterministic Nonperiodic Flow*, Journal of the Atmospheric Science, no. 130, 1963.

[2] Peter Stavroulakis, *Chaos Applications in Telecommunications*, Ed. Taylor & Francis.

[3] Claude Shannon, *A Mathematical Theory of Cryptography*, Sept. 1946.

[4] P. Colet and R. Roy, *Digital communications with chaotic lasers*, Optics Letters, vol. 19, pp. 2056-2058, 1994.

[5] C. R. Mirasso, P. Colet and P. García-Fernandez, *Synchronization of chaotic semiconductor lasers: Applications to encoded communications*, Photonics Technology Letters, vol. 8, no. 2, pp. 299-301, 1996.

[6] J. Doyne Farmer, *Chaotic attractors of an infinite-dimensional dynamical system*, Physica 4D, pp. 366-393, 1982.

[7] D. A. Russel, J. D. Hanson, and E. Ott, *Dimension of strange attractors*, Physical Review Letters, vol. 45, pp. 1175, 1980.

[8] H. Froehling, J. P. Crutchfield, D. Farmer, N. H. Packard, and R. Shaw, *On determining the dimension of chaotic flows*, Physica (Utrecht) 3D, pp. 605, 1981.

[9] H. S. Greenside, A. Wolf, J. Swift, and T. Pignataro, *Impractically of a box-counting algorithm dimensionality of strange attractors*, Physical Review Letters, A 25, vol. 3453, 1982.

[10] P. Grassberger and I. Procaccia, *Characterization of Strange Attractors*, Physical Review Letters, vol. 50, no. 5, 1983.

[11] D. Farmer, *Information Dimension and the Probabilistic Structure of Chaos*, Chapter 1, UCSC Doctoral dissertation.

[12] A. Ben Saïda, *Using the Lyapunov exponent as a practical test for noisy chaos*, Social Science Research Network SSRN, id. 970074, 2007.

[13] J. Kaplan and J. Yorke, *Functional Differential Equations and Approximation of Fixed Points*, H. O. Peitgen and H. O. Walther, Eds., pp. 228, 1979.

[14] H. Mori, *Statistical Dynamics of Chaotic Flows*, Progress in Theory Physics, vol. 63, no. 6, pp. 1931-1944, 1980.

[15] R. Vicente, J. Daudén, P. Colet, and R. Toral, *Analysis and Characterization of the Hyperchaos generated by a Semiconductor Laser subject to a Delayed Feedback Loop*, Journal of Quantum Electronics, vol. 41, no. 4, 2005.

[16] F. T. Arecchi, W. Gadomski, and R. Meucci, *Generation of chaotic dynamics by feedback on a laser*, Physical Review A (Rapid Communications), vol. 34, no. 2, 1986.

[17] I. Fischer, O. Hess, W. Elsässer, and E. Göbel, High-Dimensional Chaotic Dynamics of an External Cavity Semiconductor Laser, Physical Review Letters, vol. 73, no. 16, 1994.

[18] V. Annovazzi-Lodi et al., *Chaos-based approach to secure communications*, Optics and Photonics News, vol. 19, issue 10, pp. 36-41, 2008.

[19] Apostolos Argyris et al., *Chaos-based communications at high bit rates using commercial fibre-optic links*, Nature Letters, vol. 437, pp. 343-346, 2005.

[20] D. Kanakidis, A. Argyris, A. Bogris, and D. Syvridis, *Influence of the Decoding Process on the Performance of Chaos Encrypted Optical Communication Systems,* Journal of Lightwave Technology, vol. 24, no. 1, 2006.

[21] R. Clavero, F. Ramos, and J. Martí, *Bistability Analysis for Optical Flip-Flops based on a SOA-MZI with Feedback*, Journal of Lightwave Technology, vol. 25, no. 11, 2007.

[22] R. Clavero, F. Ramos, and J. Martí, *All-optical flip-flop based on an active Mach-Zehnder interferometer with a feedback loop*, Optics Letters, vol. 30, no. 21, 2005.

[23] G. P. Agrawal and N. A. Olsson, *Self-phase modulation and spectral broadening of optical pulses in semiconductor laser amplifiers*, Journal in Quantum Electronics, vol. 25, no. 11, pp. 2297-2306, 1989.

[24] P. Glendinning, *Stability, Instability and Chaos: An Introduction to the Theory of Nonlinear Differential Equations,* Cambridge Univ. Press, 1994.

[25] S. H. Strogatz, *Nonlinear Dynamics and Chaos: With Applications to Physics, Biology, Chemistry, and Engineering*, Studies in Nonlinearities, Westview Press, 2001.